Original Article

Institution of MECHANICAL ENGINEERS

Journal of MECHANICAL ENGINEERING SCIENCE

Proc IMechE Part C:
J Mechanical Engineering Science
2021, Vol. 235(6) 963–974

DOI: 10.1177/0954406220939104
journals.sagepub.com/home/pic
SAGE

Crashworthiness optimization of hierarchical hexagonal honeycombs under out-of-plane impact

M Altin[1], E Acar[2] and MA Güler[3]

Abstract

This paper presents a numerical study of regular and hierarchical honeycomb structures subjected to out-of-plane impact loading. The specific energy absorption capacity of honeycomb structures via nonlinear explicit finite element analysis is investigated. The constructed finite element models are validated using experimental data available in the literature. The honeycomb structures are optimized by using a surrogate-based optimization approach to achieve maximum specific energy absorption capacity. Three surrogate models polynomial response surface approximations, radial basis functions, and Kriging models are used; Kriging models are found to be the most accurate. The optimum specific energy absorption value obtained for hierarchical honeycomb structures is found to be 148% greater than that of regular honeycomb structures.

Keywords

Crashworthiness, honeycomb, optimization, specific energy absorption, surrogate model

Date received: 4 April 2020; accepted: 8 June 2020

Introduction

Honeycomb thin-walled structures are well known for their significant energy absorption capacity and light weight. These structures are used in bumpers as crash boxes to absorb energy by deforming plastically and thereby protecting passengers against high inertial forces during accidents. Studies evaluating the crashworthiness of honeycomb structures were initiated by McFarland.[1] In recent years, honeycomb materials have been employed in automotive,[2–4] railway,[5–7] ship[8–10] and aerospace structures.[11–13]

In honeycomb structures, hierarchy is known to improve the mechanical properties. These structures can be made from aluminum,[14–16] composite,[17–19] or steel.[17,20,21] In the literature, there exist numerous experimental and numerical studies on the in-plane and out-of-plane crashworthiness assessment of honeycomb structures.

The in-plane crash analysis of honeycomb structures includes the following: crashworthiness of honeycomb structures were examined under in-plane uniaxial loading experimentally and numerically.[22–25] Ganilova et al.[26] considered hybrid bumper-crush can design composed of a negative-stiffness honeycomb, the recoverable structure and the honeycomb-filled elements. They evaluated the performance of this design through finite element modeling, using ANSYS, and found that the honeycomb-filled tubes outperform the empty tubes in terms of Specific Energy Absorption (SEA). Chen et al.[27] explored the energy absorption capacity of hierarchical honeycomb structures in which triangular lattice configurations were used as cell walls of regular honeycombs. They produced these hierarchical structures with a commercial 3D printer, and found that the structural hierarchy improved the energy absorption capacity under in-plane loading conditions.

Out-of-plane crashworthiness of honeycomb structures can also be improved via hierarchy. Li et al.[21] studied the energy absorption efficiency of regular hexagonal single-cell and hierarchical hexagonal multi-cell tubes through experimental and numerical studies. They found that the SEA of the hierarchical multi-cell tube was 136% greater than that of the single-cell tube. Sun et al.[28] investigated the effect of

[1]Department of Automotive Engineering, Gazi University, Ankara, Turkey
[2]Department of Mechanical Engineering, TOBB University of Economics and Technology, Ankara, Turkey
[3]College of Engineering and Technology, American University of the Middle East, Kuwait

Corresponding author:
E Acar, Department of Mechanical Engineering, TOBB University of Economics and Technology, Ankara, Turkey.
Email: acar@etu.edu.tr

using a vertex-based hierarchy on the mechanical properties of honeycomb structures under axial out-of-plane dynamic loading. They incorporated the concept of hierarchical (regular, first-order, and second-order) structures under out-of-plane loading. They observed that first-order and second-order hierarchical honeycomb structures could improve the SEA by more than 81.3% and 185.7%, respectively.

Even though there exists substantial number of studies on the crashworthiness optimization of regular honeycomb structures (including the references[29–31]), to the best of the authors' knowledge, there is no research study on the crashworthiness optimization of hierarchical hexagonal honeycombs. The main contribution of the present study is to perform crashworthiness optimization of a hierarchical hexagonal honeycomb structure for the first time in the literature. In this study, these structures are first optimized to obtain the maximum SEA, and the optimum SEA values of regular and first-order hierarchical hexagonal honeycomb structures are then compared using a nonlinear explicit finite element code in LS-DYNA.

This paper is structured as follows: In the Geometric characteristics of hierarchical hexagonal honeycombs section, the geometrical characteristics of the hierarchical hexagonal honeycomb structures are presented. In the Crash evaluation metrics section, crash evaluation metrics are defined. The development of finite element models and their validation with experimental results from the literature are presented in the Finite element modelling section. In the Surrogate-based optimization section, the optimization problem formulations of the regular and first-order hierarchical hexagonal honeycomb structures are provided. The optimization results are presented and discussed in the Optimization results section, followed by the conclusions in the Concluding remarks section.

Geometric characteristics of hierarchical hexagonal honeycombs

In this study, hierarchical hexagonal honeycomb (HHH) structures were obtained by replacing the corners of regular hexagonal honeycomb (RHH) structures with smaller hexagons, as in Ajdari et al.[32] The geometric details of the RHH and HHH structures are shown in Figure 1. Note that only first-order hierarchy is considered in this study, whereas the consideration of higher-order hierarchies remains the scope of a future study.

In this study, the oblique wall angle, θ, of the HHH structures varied from 15° to 75°. The HHH structures with different oblique wall angle values are shown in Figure 2.

The first-order edge length of the HHH structures (L_{f1}) can be related to the edge length of the RHH structures (L_r) through the structural organization

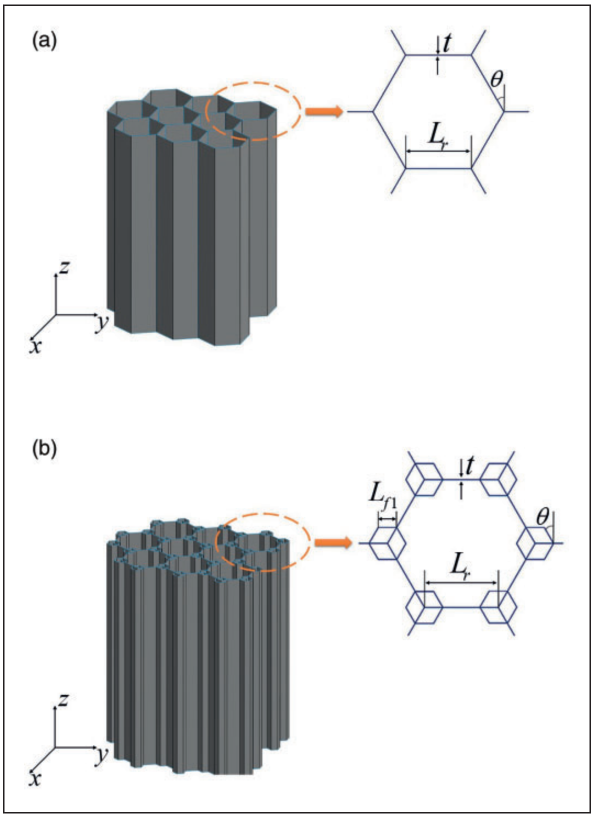

Figure 1. Geometric details of the (a) regular hexagonal honeycomb (RHH) and (b) hierarchical hexagonal honeycomb (HHH).

parameter, $\gamma = L_{f1}/L_r$.[33] In this study, the structural organization parameter, γ, was varied from 0.05 to 0.30. The HHH structures with different γ values are shown in Figure 3.

Crash evaluation metrics

The crashworthiness performance of a structure can be evaluated by means of several evaluation metrics. Such crash assessment metrics are used in the initial design stages of energy absorbing systems. Those metrics include the total energy absorbed, $E_{absorbed}$, peak crush force, F_{peak}, mean crush force, F_{mean}, crush force efficiency, CFE, and specific energy absorption, SEA.[34,35] The explanation of these metrics can be given as follows.

Total energy absorbed

The total energy absorbed ($E_{absorbed}$) in a crash equals the area under the force-displacement curve. It is defined as

$$E_{absorbed} = \int P \mathrm{d}\delta \tag{1}$$

where P and δ are the crushing force and the corresponding displacement, respectively.

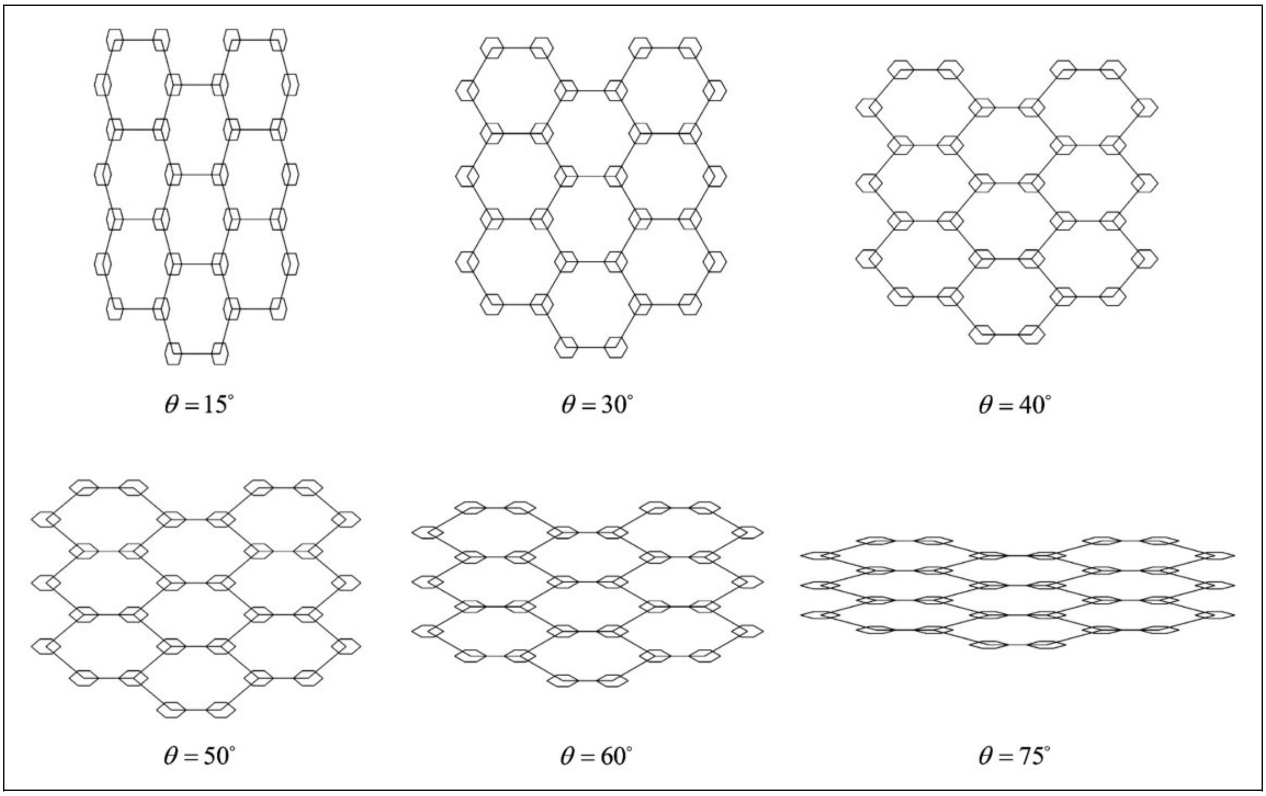

Figure 2. Top view of HHH structures with different oblique wall angles for $\gamma = 0.2$.

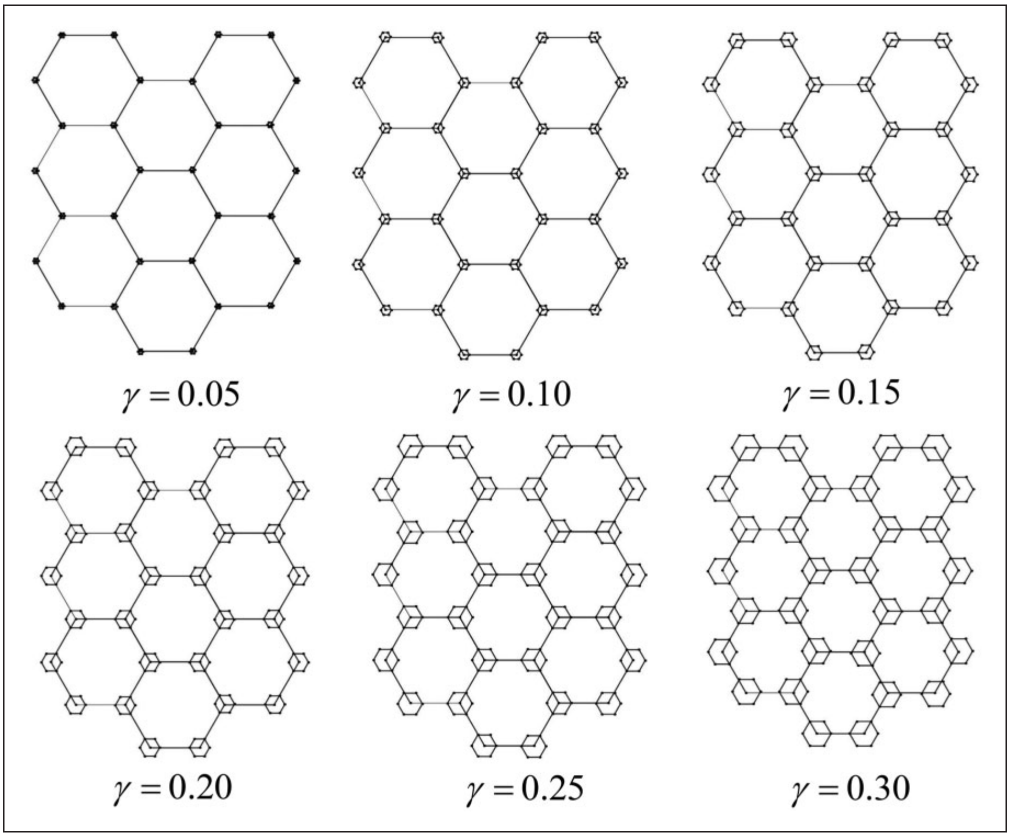

Figure 3. Top view of HHH structures with different γ values for $\theta = 30^o$.

Peak crush force

Peak crush force (F_{peak}) is a critical parameter during the impact of a crash absorbing structure and defined as the peak force in the force–displacement curve.

Mean crush force

The mean crush force (F_{mean}) can be determined by dividing the total energy absorbed ($E_{absorbed}$) by the total displacement (Δ), and is given by

$$F_{mean} = \frac{E_{absorbed}}{\Delta} \quad (2)$$

Note that Δ is the crushing displacement of the rigid wall.

Crush force efficiency

Crash force efficiency (CFE) is another indicator in relation to the crashworthiness performance, and it can be defined as

$$CFE = \frac{F_{mean}}{F_{peak}} \quad (3)$$

Specific energy absorption

Specific energy absorption (SEA) can be defined as the ratio of the total energy absorbed over the mass of a crash absorbing structure (m).

$$SEA = \frac{E_{absorbed}}{m} \quad (4)$$

In this study, the performances of the RHH and HHH structures are evaluated based on SEA, and the optimization of these structures is performed to achieve the maximum SEA.

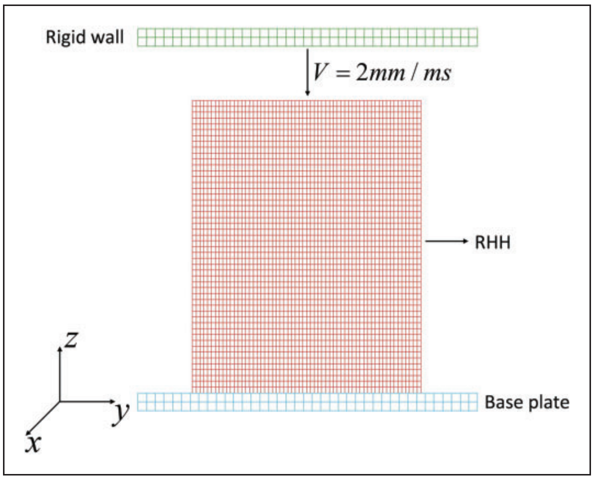

Figure 4. Finite element model of the RHH structure, the rigid wall, and the base plate.

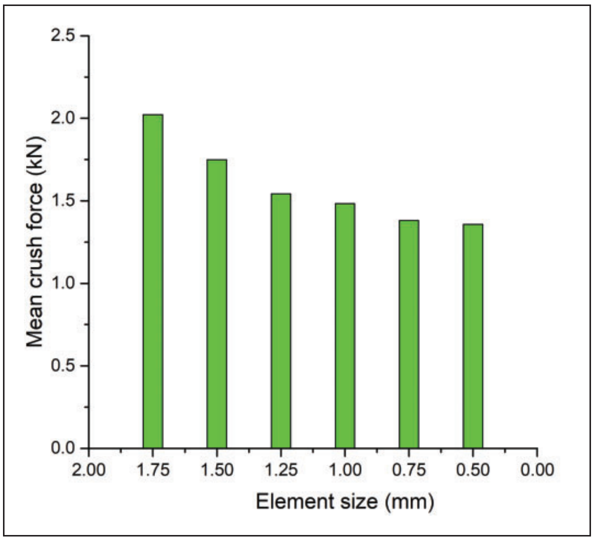

Figure 5. Variation of mean crush force for various element sizes.

Finite element modeling

FE model of RHH structures

The FE software LS-DYNA with explicit time integration is employed to perform numerical analysis. A schematic figure representing the finite element model of an RHH structure under out-of-plane loading conditions is shown in Figure 4. The RHH structure, rigid wall (impactor), and base plate are discretized using Belytschko-Tsay reduced-integration thin-shell elements with five integration points across the thickness. To determine the appropriate element size, a mesh convergence study is performed based on the variation of the mean crush force (see Figure 5). The element size of 0.75 mm is found to be suitable; hence, it is used throughout the simulations. Figure 6 shows an isometric view of the finite element mesh of the RHH structure.

The RHH structures are made of AA3003 H18, whose density is $\rho = 2700\,kg/m^3$, Young's modulus $E = 69$ GPa, initial yield stress $\sigma_y = 115$ MPa, ultimate stress $\sigma_u = 154$ MPa, and Poisson's ratio $\nu = 0.33$. The stress–strain behavior used in this study (AA3003 H18) is given in Table 1.[14]

The dynamic and static coefficients of frictions are taken as 0.2 and 0.3, respectively, based on our earlier works and others.[36–38] The material model MAT 24, "MAT_PIECEWISE_LINEAR_PLASTICITY", in LS-DYNA was adopted to model the RHH structures. The rigid wall and the base plate is modeled with MAT 20 ("MAT_RIGID" in LS-DYNA). The quasi-static out-of-plane compressive load is applied by the rigid wall moving at a constant speed of 2 mm/ms using the command "BOUNDARY_PRESCRIBED_MOTION_RIGID". The self-contact of the RHH structures is modeled with the "CONTACT_AUTOMATIC_SINGLE_SURFACE" contact type. The contact between the HHH and the rigid wall is modeled by using the "CONTACT_AUTOMATIC_NODES_TO_SURFACE" type.

Validation of the FE Model of the RHH structures

The FE model described in the previous section is validated using the experimental results of Zhang et al.,[14] where AA3003 H18 RHH structures were tested under out-of-plane loading conditions. In the validation process, FE models of a 3×3-unit cell and 5×5-unit cell, each with a wall length of $L_r = 6$ mm and thickness of $t = 0.075$ mm, are generated. The comparison of our FE analysis results with the experimental results of Zhang et al.[14] in terms of load-displacement curves and collapse modes are shown in Figures 7 and 8, respectively. Moreover, the total energy absorption prediction of our FE model was compared with the corresponding experimental result of Zhang et al.,[14] as shown in Table 2. Overall, the validation results demonstrate good compatibility between the numerical results of our FE model and the experimental results of Zhang et al.[14]

FE model of HHH structures

The FE model of HHH structures has the same material model, boundary conditions, and contact definitions as those of the RHH structures, as explained in the FE model of RHH structures section. However, a different edge length value is used for the HHH structures. In order to have a wide range of γ values, the edge length is taken as $L_r = 20$ mm. The mesh size used in the FE model of RHH structures was taken as 0.75 mm, based

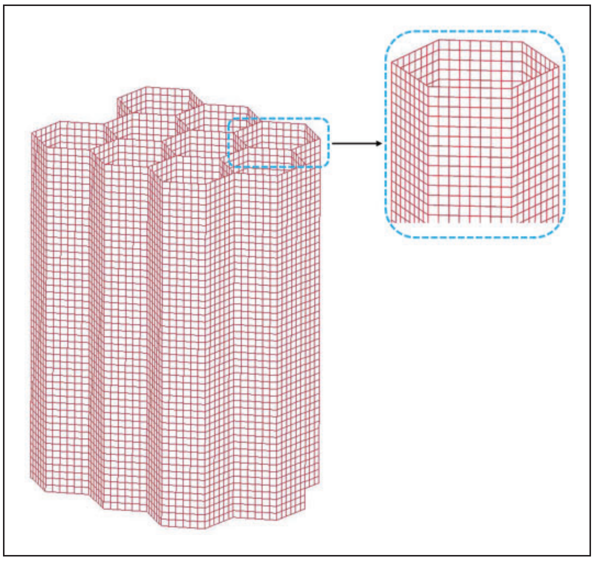

Figure 6. Isometric view of the finite element mesh of the RHH structure.

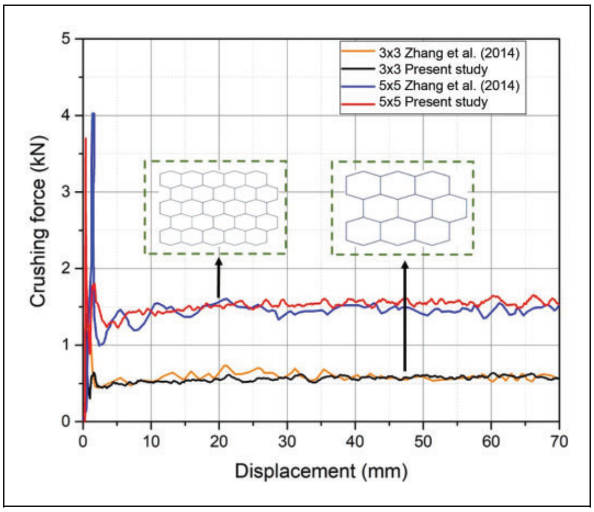

Figure 7. Comparison of the crushing force–displacement curves obtained from FE simulations with the experimental results of Zhang et al.[14]

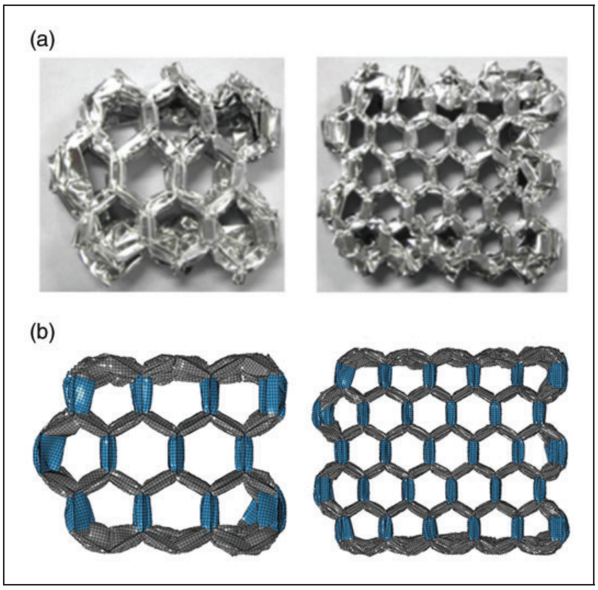

Figure 8. Comparison of the progressive collapse: (a) experimental result of Zhang et al.[14]; (b) FE simulation results of this study.

Table 1. True stress–true effective plastic strain data points used in the finite element analysis simulation for AA3003 H18.[14]

σ_t [MPa]	115	127	153	174	201	260	0.298	0.351
ε_p [%]	0.0	0.045	0.097	0.145	0.220	0.418	0.542	0.695

on the mesh convergence study (see Figure 5). Similarly, the mesh size in the FE model of the HHH structures is also intended to be as close as possible to 0.75 mm; however, the mesh size differs according to the γ parameter. For instance, when the structural organization parameter, γ becomes 0.05, the side length of each hexagon becomes $L_{f1} = 1$ mm, and the mesh size becomes 0.5 mm, such that there are two elements per hexagonal side as shown in Figure 9. However, when $\gamma = 0.30$, the side length of hexagon becomes $L_r = 6$ mm, and the mesh size is taken as 0.75 mm, such that there are eight elements per hexagonal side, as shown in Figure 10.

Table 2. Comparison of total energy absorption results.

Cell configuration	Present study FE results	Experimental result of Ref.[14]	Error %
3×3	39.45 J	39.05 J	1.01
5×5	105.81 J	100.01 J	5.79

Surrogate-based optimization

For the RHH structures, the design optimization problem to achieve maximum SEA can be expressed as

$$\begin{aligned} &Find \quad \theta, t \\ &Min \quad -SEA\ (\theta, t) \\ &s.t. \quad 15^\circ \leqslant \theta \leqslant 75^\circ, 0.05\ \text{mm} \leqslant t \leqslant 0.15\ \text{mm} \end{aligned} \tag{5}$$

where θ and t are depicted earlier in Figure 1(a).

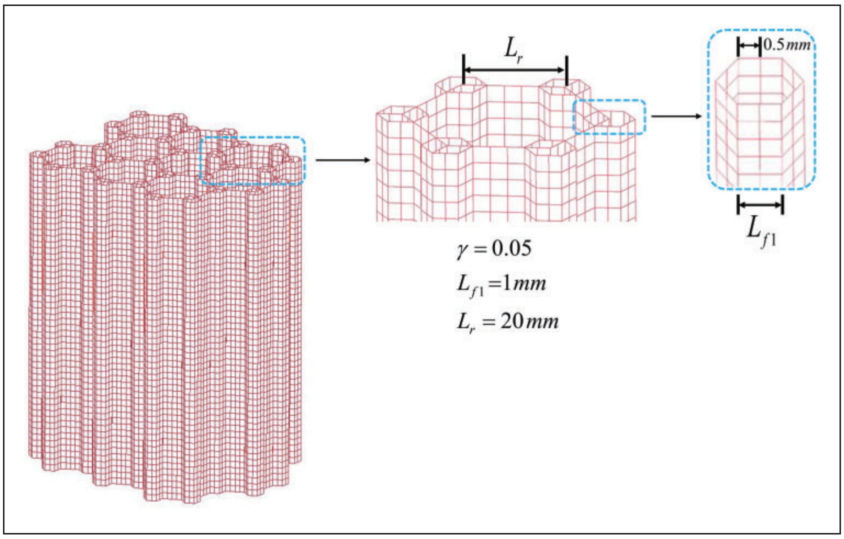

Figure 9. Isometric view of the FE mesh of the HHH structures when $\gamma = 0.05$.

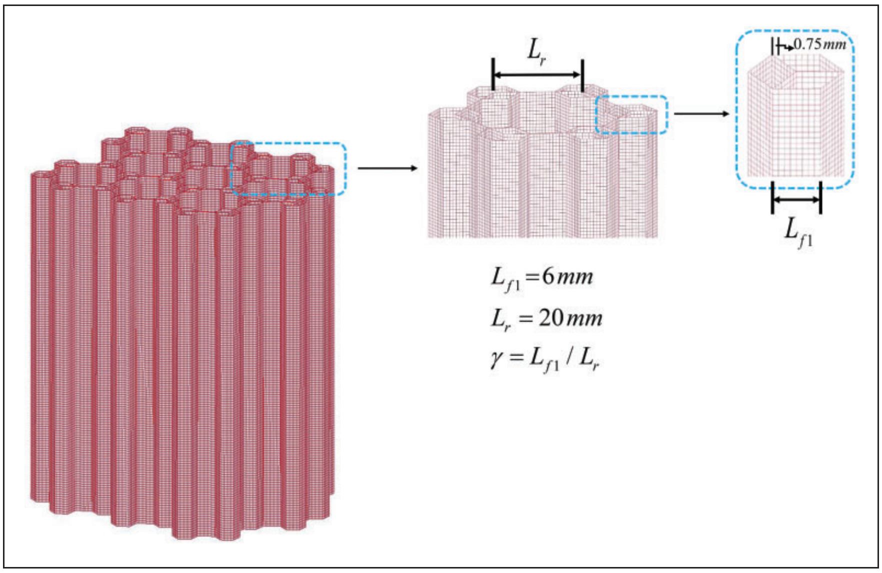

Figure 10. Isometric view of the FE mesh of the HHH structures when $\gamma = 0.30$.

Similarly, for the HHH structures, the design optimization problem for maximum SEA can be stated as

$$\begin{aligned} &Find && \theta, t, \gamma \\ &Min && -SEA(\theta, t, \gamma) \\ &s.t. && 15^\circ \leqslant \theta \leqslant 75^\circ, 0.05\ \text{mm} \leqslant t \leqslant 0.15\ \text{mm} \\ & && 0.05 \leqslant \gamma \leqslant 0.30 \end{aligned} \tag{6}$$

where γ, θ and t are depicted earlier in Figure 1(b).

The solution of these problems requires calculation of the SEA values many times during optimization. As the computational cost associated with the SEA calculation is high, a surrogate-based optimization approach is used as in earlier works.[39–41] In this approach, a pool of training (data) points is first generated through design of experiments (DOE) technique. Next, the corresponding outputs are calculated at the data points. Then, the data points and the corresponding outputs are used to generate the surrogate model. Finally, the constructed surrogate models are incorporated into an optimizer to obtain the optimum design.

In this study, the *ga* built-in optimizer of MATLAB that uses genetic algorithm[42] is used. The population size is taken 100, the elite count is taken 6, the crossover fraction is taken 80%, the maximum number of generations is taken 300, and remaining algorithms parameters are taken as the default values in MATLAB.

Design of experiments

In this study, Latin hypercube sampling is employed to obtain the training points. The MATLAB built-in function *lhsdesign* with *maximin* criterion (to maximize the minimum distance between the training points) is used, where the maximum number of iterations is set to 1000. Note that the classical designs such as Box-Behnken design (BBD) and factorial designs (FD) could have been used in this study. However, Latin hypercube sampling (LHS) has some advantages over these classical designs. LHS allows flexible sample sizes and has a good space filling capability that helps it representing the design space with relatively small number of sample points. The number of sampling points required for an FFD is exponentially proportional to the dimensionality of the problem, and BBD has poor space filling capability compared to LHS.

The bounds of the input variables for the RHH and HHH structures are given in the optimization problem statements (see equations (5) and (6)). The number of training points is chosen as 10 times the number of input variables as suggested by Jones et al.[43] Therefore, 20 and 30 training points are generated for the RHH and HHH structures, respectively.

Sensitivity analysis

Before constructing the surrogate models, a global sensitivity analysis based on the Sobol indices method[44] is performed. Sobol indices method is a variance-based method that measures the importance of an input variable based on its effect on the response variance. The main shortcoming of this method is the requirement of a large number of model evaluations. To reduce the computational cost of the Sobol indices method, Gaussian processes regression model-based approach[45] is used. The first-order and total Sobol indices of each variable are provided for SEA in Figure 11. It is seen that the oblique wall angle θ is the most important variable influencing SEA.

The comparison of the first-order and total sensitivity indices as well as the summation of the first-order indices can be used to evaluate the presence of the interactions between input variables. Figure 11 shows that the first-order indices and the total sensitivity indices are close to each other, and the summation of the first-order sensitivity indices are close to 1, thereby indicating that the interaction between the input variables are small.

Accuracy of the surrogate models

Quadratic polynomial response surface (PRS) approximations, radial basis functions (RBF) with multiquadratic formulation, and a Kriging model (KR1) with linear trend and Gaussian correlation models were used to relate the SEA to the input variables. A brief overview of the mathematical formulations of the PRS, RBF, and KR1 models can be found in Appendix B of Acar et al.[39]

The leave-one-out generalized-mean-square cross-validation error metric, $GMSE$ is used to asses the accuracies of the generated surrogate models. $GMSE$ is computed from

$$GMSE = \sqrt{\frac{1}{N}\sum_{k=1}^{N}\left(\hat{y}_k^{(-k)} - y_k\right)^2} \tag{7}$$

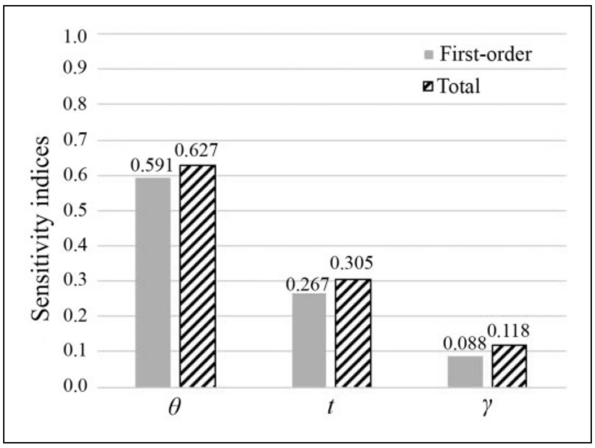

Figure 11. First-order and total Sobol sensitivity indices for SEA.

where N is the number of training points, $\hat{y}_k^{(-k)}$ is the prediction of the response obtained from the surrogate model which is constructed by using all data points excluding the kth data point, and y_k is the response at the kth data point.

A normalized version of $GMSE$ ($GMSE_{nor}$) is usually used instead of $GMSE$ itself. $GMSE_{nor}$ can be computed from

$$GMSE_{nor} = \frac{GMSE}{\frac{1}{N}\sum_{k=1}^{N} y_k} \tag{8}$$

Table 3. Normalized GMSE values of the surrogate models constructed for predicting the SEA of the RHH and HHH structures.

Surrogate model	Regular	Hierarchical
PRS	7.7	6.8
RBF	11.3	20.5
KR1	**6.5**	**6.6**

Note: The smallest errors are shown in bold letters.

Table 3 provides the normalized $GMSE$ values of the surrogate models constructed for predicting the SEA of the RHH and HHH structures. KR1 is found to be superior to both PRS and RBF in terms of SEA prediction accuracy. The normalized $GMSE$ of the KR1 model is 6.5% for the RHH structures, and 6.6% for the HHH structures. The mentioned values are acceptable to predict SEA which is a highly nonlinear response.

Optimization with multiple surrogate models

In an earlier study, it is found that the optimum solution is not necessarily obtained by using the most

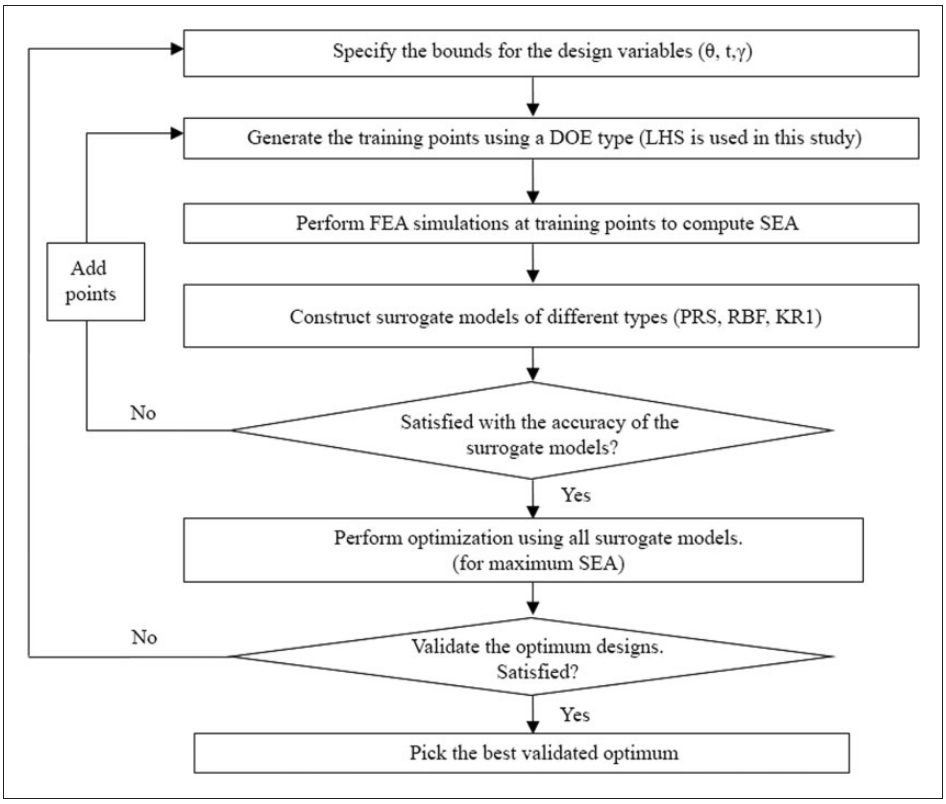

Figure 12. Surrogate-based approach for optimization of the honeycomb structures.

Table 4. Optimization results for maximum SEA of the RHH structures.

Surrogate model	θ (deg)	t (mm)	SEA via surrogate[a]	SEA via FEA[a]	% error
PRS	20.0	0.138	6.56	6.51	0.8
RBF	15.0	0.149	6.99	6.55	6.7
KR1	25.5	0.150	6.88	**6.84**	0.7

Note: The maximum SEA value obtained via FEA is shown in bold font. FEA: finite element analysis.
[a]SEA is in kJ/kg.

Table 5. Optimization results for maximum SEA of the first-order HHH structures.

Surrogate model	θ (deg)	t (mm)	γ	SEA via surrogate[a]	SEA via FEA[a]	% error
PRS	25.3	0.15	0.211	17.79	16.93	5.1
RBF	37.9	0.15	0.050	18.67	11.52	62.1
KR1	15.0	0.15	0.182	17.26	**16.97**	1.7

Note: The maximum SEA value obtained via FEA is shown in bold font. FEA: finite element analysis.
[a]SEA is in kJ/kg.

accurate surrogate model.[39] Therefore, the honeycomb structures are optimized by using different surrogate model types and the design with the optimum performance is determined. Finally, the performance of the optimum design is validated using LS-DYNA. The surrogate-based optimization framework used in this study is depicted in Figure 12.

Optimization results

Table 4 shows the optimization results for the maximum SEA of the RHH structures. It can be observed that the optimum design predicted by the KR1 model led to the largest SEA value, and the error in SEA prediction was only 0.7%. The optimum designs predicted by the other surrogate models resulted in smaller SEA values and larger errors in SEA prediction.

Table 5 shows the optimization results for maximum SEA of the HHH structures. It can be observed that the optimum design predicted by the KR1 model led to the largest SEA value, and the error in SEA prediction is only 1.7%. The optimum designs predicted by the other surrogate models exhibited smaller SEA values and larger errors in SEA prediction.

Comparing the optimization results presented in Tables 4 and 5, the optimum oblique wall angle is found to be $\theta = 15°$, which is the lower bound for this parameter, for the HHH structures, whereas that of the RHH structures is found to be $\theta = 25.5°$. The optimum wall thickness is found to be $t = 0.15$ mm, the upper bound for this parameter in both the RHH and HHH structures. The optimum value of the structural organization parameter is found to be $\gamma = 0.182$, which lies almost directly between its lower and upper bounds of 0.05 and 0.30. Finally, it is also observed that the SEA of the optimum HHH structure is 148% larger than that of the optimum RHH structure.

The effect of the design variables on the crash performance of HHH structure is further investigated by changing each design variable one at a time around the optimum design configuration. The oblique wall angle, the wall thickness, and the structural organization parameter are changed between 15° and 75°, 0.05–0.15 mm, 0.05–0.3, respectively. Figure 13(a) shows that the absorbed energy as well as the mean crush force reduces as the oblique wall angle increases. Since the oblique wall angle does not affect the mass, SEA also reduces as the oblique

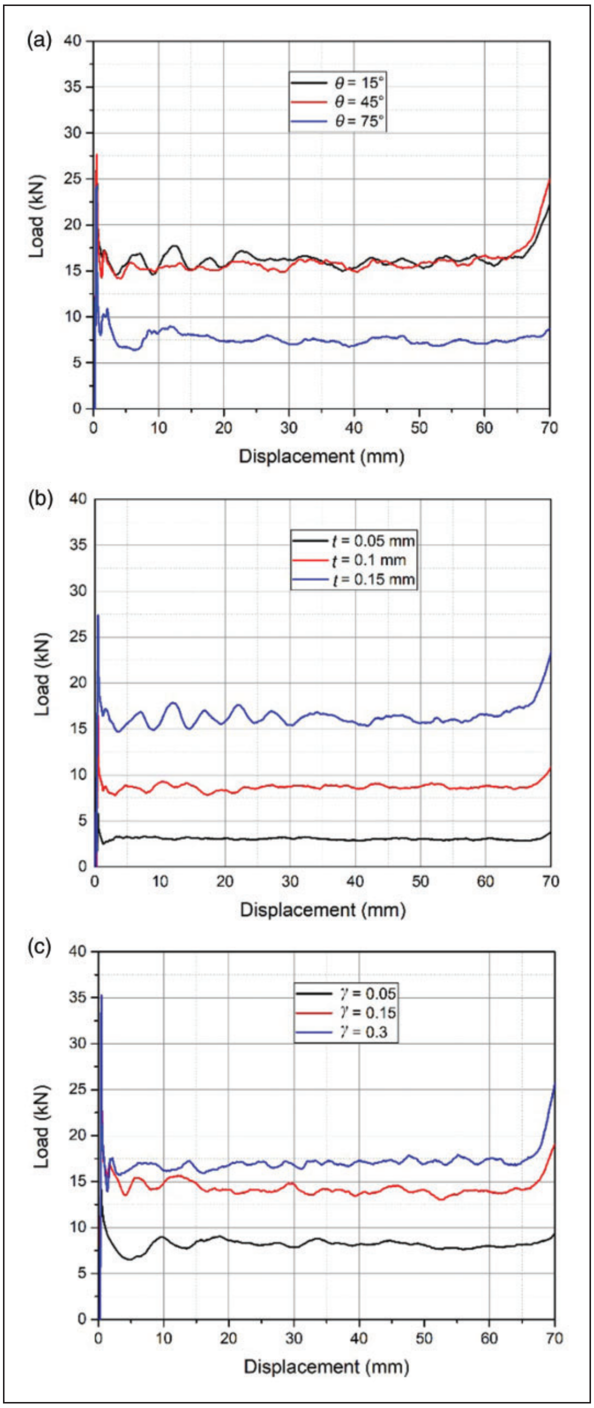

Figure 13. Effect of design variables on the crash performance of HHH structures (around the optimum design configuration). (a) Effect of θ, $t = 0.15$ mm and $\gamma = 0.182$ (b) Effect of t, $\theta = 0.15°$ and $\gamma = 0.182$ (c) Effect of γ, $\theta = 0.15°$ and $t = 0.15$

wall angle increases. Figure 13(b) shows that the absorbed energy as well as the mean crush force increases as the wall thickness increases, as expected. It is found that the rate of increase in the absorbed energy is larger than the rate of increase in the mass due to increased thickness; hence, SEA increases as the oblique wall angle increases. Figure 13(c) shows that the absorbed energy as well as the mean crush force increases as the structural organization parameter increases. Note also that the mass also increases as the structural organization parameter (γ) increases. It is found that SEA increases as γ increases from 0.05 to 0.182, but then SEA reduces as γ increases further from 0.182 to 0.30.

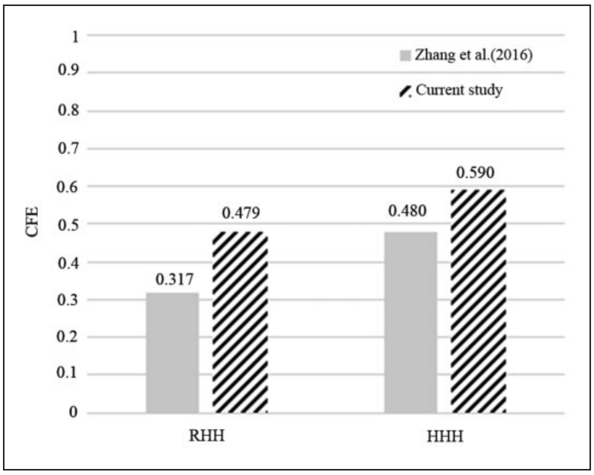

Figure 14. Comparison of CFE values obtained from the current study with those in the literature.

The CFE values of the optimum RHH and HHH structures are also investigated. The CFE value of the optimum RHH structure is found to be 0.479, whereas that of the optimum HHH structure is found to be 0.590 (see Figure 14). The CFE value obtained for the RHH structure is 51% larger than those reported in the literature (see Table 3 of Zhang et al.[33]). Similarly, the CFE value obtained for the HHH structure is 23% larger than those reported in the literature (see Table 3 of Zhang et al.[33]).

Figure 15 compares progress of deformation for the optimum HHH structure with that of the RHH structure. It can be seen that progressive collapse of the HHH structure is much better than that of RHH structure.

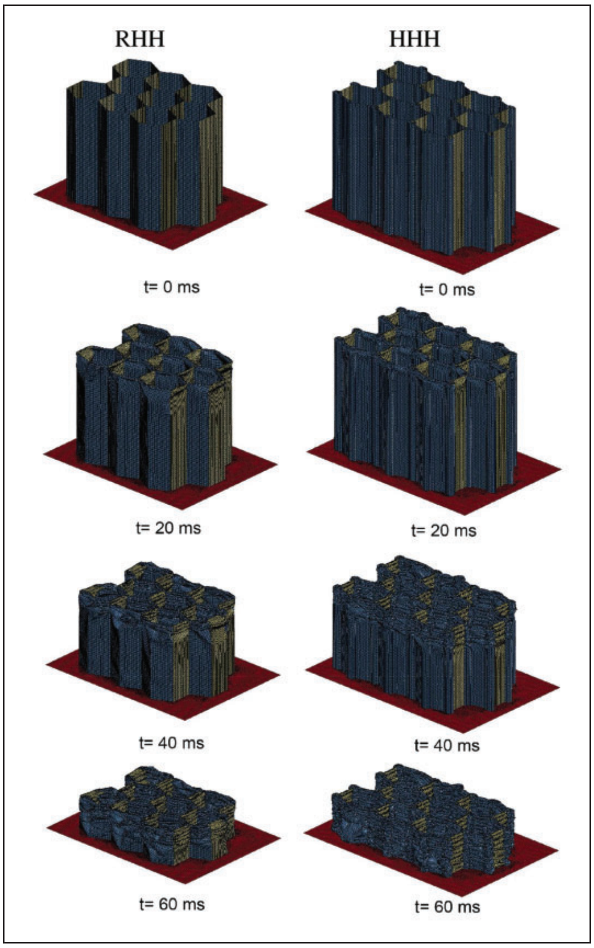

Figure 15. Deformation process of the optimum HHH structure.

Concluding remarks

This study explored the crashworthiness performance of RHH and HHH structures under out-of-plane impact loading. Several geometrically different honeycomb structures were evaluated using a finite element model, which was validated against experimental results available in the literature. A surrogate-based optimization approach was then used to maximize the SEA of the honeycomb structures. The following conclusions were drawn from the results of this study:

- Multiple surrogate models (PRS, RBF, and KR1) were used for SEA prediction, the most accurate of which was found to be the Kriging model for both the RHH and HHH structures.
- The optimum oblique wall angle of the HHH structures was found to be $\theta = 15^\circ$, which was the lower bound for this parameter, whereas that of the RHH structures was found to be $\theta = 25.5^\circ$.
- The optimum wall thickness was found to be $t = 0.15$ mm, the upper bound for this parameter for both the RHH and HHH structures.
- The optimum value of the structural organization parameter was found to be $\gamma = 0.182$, which lies almost directly between its lower and upper bounds of 0.05 and 0.30.
- The SEA of the optimum HHH structure was 148% larger than that of the optimum RHH structure.
- The CFE value obtained for the optimum RHH structure was found to be 51% greater than those reported in the literature.

- Similarly, the CFE value obtained for the optimum HHH structure was found to be 23% larger than those reported in the literature.

In this study, only first-order hierarchical structures are considered. Investigation of upper level hierarchies remains the scope of future work. It is also noted that for a crashworthy design, the designer need to ensure the safety aspects of the structure, usually considered by minimizing the peak crush force[46,47] or maximizing the crush force efficiency.[34,39] It is accepted that this is missing in the present study and opt to extend this work to a multi-objective optimization study by including the peak crush force or crush force efficiency as a second objective.

Declaration of Conflicting Interests

The author(s) declared no potential conflicts of interest with respect to the research, authorship, and/or publication of this article.

Funding

The author(s) received no financial support for the research, authorship, and/or publication of this article.

ORCID iDs

E Acar https://orcid.org/0000-0002-3661-5563
MA Güler https://orcid.org/0000-0002-1159-556X

References

1. Mc Farland R. Hexagonal cell structures under post-buckling axial load. *AIAA J* 1963; 1: 1380–1385.
2. Niknejad A, Liaghat G, Moslemi Naeini H, et al. A theoretical formula for predicting the instantaneous folding force of the first fold in a single cell hexagonal honeycomb under axial loading. *Proc IMechE, Part C: J Mechanical Engineering Science* 2010; 224: 2308–2315.
3. Wu Y, Fang J, He Y, et al. Crashworthiness of hierarchical circular-joint quadrangular honeycombs. *Thin-Wall Struct* 2018; 133: 180–191.
4. Kang H and Kim J. Damage mitigation of a steel column subjected to automobile collision using a honeycomb panel. *J Performance Construct Facilities* 2020; 34: 04019107.
5. Yang C, Xu P, Yao S, et al. Optimization of honeycomb strength assignment for a composite energy-absorbing structure. *Thin-Wall Struct* 2018; 127: 741–755.
6. Xu P, Xing J, Yao S, et al. Energy distribution analysis and multi-objective optimization of a gradual energy-absorbing structure for subway vehicles. *Thin-Wall Struct* 2017; 115: 255–263.
7. Yao S, Xiao X, Xu P, et al. The impact performance of honeycomb-filled structures under eccentric loading for subway vehicles. *Thin-Wall Struct* 2018; 123: 360–370.
8. Crupi V, Epasto G and Guglielmino E. Comparison of aluminium sandwiches for lightweight ship structures: Honeycomb vs. foam. *Marine Struct* 2013; 30: 74–96.
9. Zhang Z, Chen Y, Hua H, et al. Crush dynamics of rubber tube under low velocity impact. *Proc IMechE, Part C: J Mechanical Engineering Science* 2014; 228: 426–440.
10. Li Y, Zhang Y, Guo K, et al. Repeated impact responses of honeycomb sandwich panels. In: *22nd International conferemce on composite materials (ICCM22)*, Melbourne, Australia, 2019, pp.2632–2634. Melbourne, VIC: Engineers Australia.
11. Campbell FC Jr . *Manufacturing technology for aerospace structural materials*. Amsterdam, the Netherlands: Elsevier, 2011.
12. Zhang H, Zheng Q, Yue G, et al. Numerical analysis of flows and aerodynamic forces in honeycomb and labyrinth seals. *Proc IMechE, Part C: J Mechanical Engineering Science* 2013; 227: 1965–1979.
13. Fiesler Saxena I, Guzman N, Hui K, et al. Disbond detection in a composite honeycomb structure of an aircraft vertical stabilizer by fiber bragg gratings detecting guided ultrasound waves. *Proc IMechE, Part C: J Mechanical Engineering Science* 2017; 231: 3001–3010.
14. Zhang X, Zhang H and Wen Z. Experimental and numerical studies on the crush resistance of aluminum honeycombs with various cell configurations. *Int J Impact Eng* 2014; 66: 48–59.
15. Fang J, Sun G, Qiu N, et al. On hierarchical honeycombs under out-of-plane crushing. *Int J Solids Struct* 2018; 135: 1–13.
16. Xu X, Zhang Y, Wang J, et al. Crashworthiness design of novel hierarchical hexagonal columns. *Compos Struct* 2018; 194: 36–48.
17. Zheng J, Zhao L and Fan H. Energy absorption mechanisms of hierarchical woven lattice composites. *Compos Part B: Eng* 2012; 43: 1516–1522.
18. Fan H, Qu Z, Xia Z, et al. Designing and compression behaviors of ductile hierarchical pyramidal lattice composites. *Mater Des* 2014; 58: 363–367.
19. Fan H, Jin F and Fang D. Mechanical properties of hierarchical cellular materials. Part I: Analysis. *Compos Sci Technol* 2008; 68: 3380–3387.
20. Sun F, Lai C, Fan H, et al. Crushing mechanism of hierarchical lattice structure. *Mech Mater* 2016; 97: 164–183.
21. Li W, Luo Y, Li M, et al. A more weight-efficient hierarchical hexagonal multi-cell tubular absorber. *Int J Mech Sci* 2018; 140: 241–249.
22. Papka SD and Kyriakides S. Experiments and full-scale numerical simulations of in-plane crushing of a honeycomb. *Acta Materialia* 1998; 46: 2765–2776.
23. Papka SD and Kyriakides S. In-plane crushing of a polycarbonate honeycomb. *Int J Solids Struct* 1998; 35: 239–267.
24. Papka S and Kyriakides S. Biaxial crushing of honeycombs:—part 1: Experiments. *Int J Solids Struct* 1999; 36: 4367–4396.
25. Papka S and Kyriakides S. In-plane biaxial crushing of honeycombs—: Part II: Analysis. *Int J Solids Struct* 1999; 36: 4397–4423.
26. Ganilova OA and Low JJ. Application of smart honeycomb structures for automotive passive safety. *Proc IMechE, Part D: J Automobile Engineering* 2018; 232: 797–811.
27. Chen Y, Li T, Jia Z, et al. 3d printed hierarchical honeycombs with shape integrity under large compressive deformations. *Mater Des* 2018; 137: 226–234.

28. Sun G, Jiang H, Fang J, et al. Crashworthiness of vertex based hierarchical honeycombs in out-of-plane impact. *Mater Des* 2016; 110: 705–719.
29. Yang X, Sun Y, Yang J, et al. Out-of-plane crashworthiness analysis of bio-inspired aluminum honeycomb patterned with horseshoe mesostructure. *Thin-Wall Struct* 2018; 125: 1–11.
30. Zhu G, Li S, Sun G, et al. On design of graded honeycomb filler and tubal wall thickness for multiple load cases. *Thin-Wall Struct* 2016; 109: 377–389.
31. Sun G, Li G, Stone M, et al. A two-stage multi-fidelity optimization procedure for honeycomb-type cellular materials. *Computat Mater Sci* 2010; 49: 500–511.
32. Ajdari A, Jahromi BH, Papadopoulos J, et al. Hierarchical honeycombs with tailorable properties. *Int J Solids Struct* 2012; 49: 1413–1419.
33. Zhang Y, Lu M, Wang CH, et al. Out-of-plane crashworthiness of bio-inspired self-similar regular hierarchical honeycombs. *Compos Struct* 2016; 144: 1–13.
34. Acar E, Altin M and Güler M. Evaluation of various multi-cell design concepts for crashworthiness design of thin-walled aluminum tubes. *Thin-Wall Struct* 2019; 142: 227–235.
35. Qiu N, Gao Y, Fang J, et al. Crashworthiness analysis and design of multi-cell hexagonal columns under multiple loading cases. *Finite Element Analys Des* 2015; 104: 89–101.
36. Guler MA, Cerit ME, Bayram B, et al. The effect of geometrical parameters on the energy absorption characteristics of thin-walled structures under axial impact loading. *Int J Crashworthiness* 2010; 15: 377–390.
37. Fang J, Gao Y, Sun G, et al. Dynamic crashing behavior of new extrudable multi-cell tubes with a functionally graded thickness. *Int J Mech Sci* 2015; 103: 63–73.
38. Altin M, Kil inçkaya Ü, Acar E, et al. Investigation of combined effects of cross section, taper angle and cell structure on crashworthiness of multi-cell thin-walled tubes. *Int J Crashworthiness* 2019; 24: 121–136.
39. Acar E, Guler M, Gerceker B, et al. Multi-objective crashworthiness optimization of tapered thin-walled tubes with axisymmetric indentations. *Thin-Wall Struct* 2011; 49: 94–105.
40. Acar E. Increasing automobile crash response metamodel accuracy through adjusted cross validation error based on outlier analysis. *Int J Crashworthiness* 2015; 20: 107–122.
41. Fang J, Sun G, Qiu N, et al. On design optimization for structural crashworthiness and its state of the art. *Struct Multidiscipl Optimiz* 2017; 55: 1091–1119.
42. Goldberg DE. *Genetic algorithms in search, optimization and machine learning*. Boston, MA: Addison-Wesley Longman Publishing Co., Inc., 1989.
43. Jones DR, Schonlau M and Welch WJ. Efficient global optimization of expensive black-box functions. *J Global Optimiz* 1998; 13: 455–492.
44. Sobol IM. Global sensitivity indices for nonlinear mathematical models and their Monte Carlo estimates. *Math Comput Simulat* 2001; 55: 271–280.
45. Marrel A, Iooss B, Laurent B, et al. Calculations of sobol indices for the Gaussian process metamodel. *Reliabil Eng Syst Safety* 2009; 94: 742–751.
46. Baroutaji A, Gilchrist M, Smyth D, et al. Crush analysis and multi-objective optimization design for circular tube under quasi-static lateral loading. *Thin-Wall Struct* 2015; 86: 121–131.
47. Baroutaji A, Sajjia M and Olabi AG. On the crashworthiness performance of thin-walled energy absorbers: recent advances and future developments. *Thin-Wall Struct* 2017; 118: 137–163.